

Quantify the wandering river floodplain vegetation response to hydrogeomorphology in high-latitude arid regions using MODIS-NDVI time series

Xarapat Ablat (1,2), Gaohuan Liu*(1), Qingsheng Liu*(1), Chong Huang (1)

¹State Key Laboratory of Resources and Environmental Information System, Institute of Geographic Sciences and Natural Resources Research, Chinese Academy of Sciences, Beijing 100101, China

²College of Resources and Environment, University of Chinese Academy of Sciences, Beijing 100049, China

Key words: Vegetation; Floodplain hydro-geomorphology; MODIS; Time-series NDVI; High latitude arid region; Yellow River basin

Abstract: Floodplain vegetation, hydrology and geomorphology are three major elements in arid and semi-arid regions. Although normalized difference vegetation index (NDVI) has been used extensively to characterize floodplain vegetation vigor and biomass, methods for quantifying variation responses of floodplain vegetation to hydrogeomorphology changes in different lateral zones in the arid regions are needed. In this study, the study reach was divided into four lateral zones based on its hydro-geomorphological differences, and time-series NDVI statistical indicators were used to characterize vegetation spatiotemporal changes in different lateral zones. The relationship between floodplain vegetation distributions and hydrogeomorphology diversity was analyzed. The result shows that average maximum NDVI value in regular inundation area is 0.23 higher than other lateral zones. Correlation analysis indicated that regular water inundation has significant benefit to floodplains rather than either highly frequently or extremely rare water inundations. Continuously or highly frequently inundation may cause decreased vegetation productivity. This study provides useful information for better understanding floodplain dynamics and river water resource management in the high-latitude arid-region floodplains.

Introduction

Vegetation, hydrology and geomorphology are three main regulatory elements for floodplain ecosystems in arid and semi-arid regions (Tockner and Stanford, 2002; Capon, 2003). The floodplain vegetation responded to hydrogeomorphology disturbances assigned to distinct spatial patterns in vegetation constitution and structures can reveal the changes in its hydrogeomorphology (Neuenschwander et al, 2008; Thomas et al, 2015). Investigating vegetation affected by hydro-geomorphological processes are represents the reliable way for understanding floodplain changing patterns and the better management of floodplain ecosystems (Broich, 2018).

Remote sensing provides a potential and unparalleled tool for quantifying the characteristics of floodplains in arid and semi-arid regions (Landmann et al, 2010; Sims et al, 2012). It has become one of the most common data source for monitoring different aspects of large floodplain information in dryland environments where with fewer cloudy days and a minimal tree canopies (Capon, 2005; Makkeasorn et al, 2009). This includes quantification of the extent, duration, and timing of floods (Raclot, 2006); the spatial variability, structure, and autocorrelation of topographic surfaces; mapping floodplain environments (Hamilton et al., 2007). Normalized difference vegetation index (NDVI) is until now the most used by worldwide to analyze and map differences in vegetation types and plant phenology, as well as soil moisture content and presence of above ground water table strongly affect their values (Tucker, 1979). Moreover, during the last decades, the availability of time-series of NDVI at low and medium spatial resolutions allowed us to study and gain in-depth insights for improved mapping of ecosystems and land monitoring at regional scale in relation to land use and climate changes (Azzali and Menenti, 2000; Epting et al., 2005)

Although significant process has been made from previous studies, however, there is a little known about the spatial distribution difference of vegetation response to river hydrogeomorphology from the riverbed to the edge of floodplains. The objective of this study is to quantify the spatial difference of vegetation responses to river hydrogeomorphology in the floodplains using NDVI statistical indicators derived from time-series daily MODIS-NDVI images. To address these questions, in our study, based on the floodplain hydro-geomorphological characteristics, the study reach is divided into four lateral zones in which the vegetation responses under complex floodplain hydro-geomorphological processes vary from the riverbed to the floodplain margins. Different statistical indicators of a pixel-based time-series NDVI, including peak NDVI values, frequency of NDVI values, and water inundation time were used to characterize the spatial distribution of vegetation vigor and biomass and analyze the relationships between the different vegetation distribution patterns and floodplain hydro-geomorphology.

Material and Methods

Study reach

The study reach is located in the southwestern region of Inner Mongolia, China (107° 24" E, 40° 38" N ~ 107° 26" E, 40° 39" N) and the most northern part of the Yellow River (Fig. 1B). It presents a typical arid and semi-arid inner continental climate, which characterized by less precipitation and more evaporation. Yearly mean precipitation of the study reach is 150-400 mm, and 75% of the precipitation is concentrated between June and September. During the study period, the mean annual temperature is 8.2°C, and there are 135-150 frost-free days and 3100-3300 h of sunshine per year. The floodplain has an area of 150 km². The longest part of the floodplain is 30 km, and the widest part is 5 km. It is a

57 typical wandering river floodplain, which has high geomorphological dynamics and a very gentle slope of 1/10000 (Figs.
58 1C-D).

59 The natural vegetation that covers the study area is mainly herbaceous. The vegetation types mainly consist of salt-
60 tolerant vegetation, such as *Bermuda grass*, *Suaeda salsa*, and *Sporobolus virginicus*. Vegetation growth mainly relies
61 on regular “banked up” water that caused by ice flooding in each winter. The average daily water level data were collected
62 from the Bayangaole water station that located in the upstream of the study area (40° 19' N, 107° 02' S) (Fig.9A) and
63 hydrological data obtained from the Yellow River Conservancy Commission (YRCC).

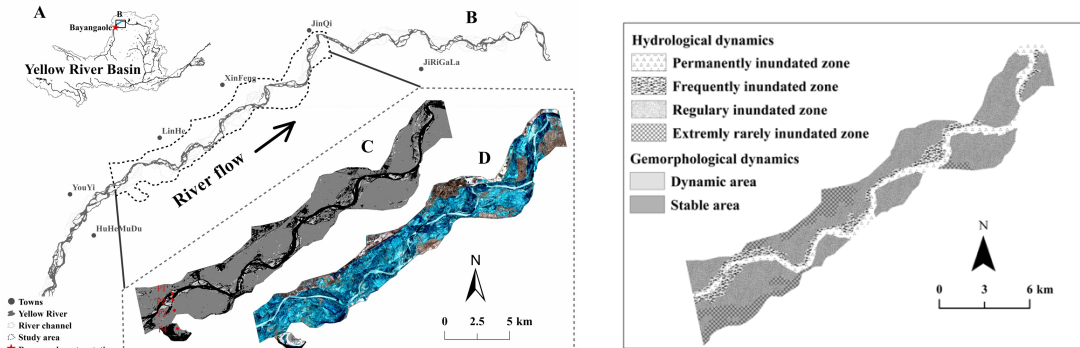


Figure 1 Location of the study area and conceptual model of hydrogeomorphological interaction patterns (A) The Yellow River Basin and location of the Linhe Reach (in black box); (B) The Linhe Reach and location of the study area (in dashed lined box); (C) NDVI image of the study reach in the 15 Aug. 2015; Pixel based points P1~P4 that located along a cross sections with different distance from riverbed. (D) False color composite image of Landsat 8 of the study area collect from 12 Jan. 2015; (E) Areas under the different hydro-geomorphological activity based on the floodplain hydro-geomorphology in the study years.

64 Lateral zonal distribution in the study reach

65 Based on the interannual hydrological dynamics of the river, the study reach was divided into four zones along the
66 main channel (Fig. 2). The division method was as follows. First, based on the indicators of hydrological analysis (IHA)
67 method, the high and low flow metrics during the 2008-2014 were determined, after which average daily flows above
68 731 m³/s in 2014 were distinguished as high flows. The frequency of each flow was calculated, and the frequencies of
69 flows in each hundred per unit were computed. The results show that flows between 1000-1100m³/s occurred on 27 days,
70 which was significantly more than other high flows. Based on the rule that these flows inundated similar areas when they
71 occurred in a single year, a Landsat 8 OLI image in 14 Aug 2014 (with an average daily flow of 1020 m³/s) was used to
72 divide the whole study reach into two zones: a highly dynamic area and a relatively static area. The highly dynamic area
73 included the continuously inundated areas and the frequently inundated floodplain areas. Based on the IHA method, the
74 extremely low flows (≤ 200 m³/s) for 2014 were calculated, and the inundation area of extremely low flows can be
75 represented by the continuously inundated areas during this year. Therefore, a Landsat 8 OLI image from 24 Apr 2014
76 (average daily flow of 209 m³/s) was used to classify the highly dynamic area into two zones: a continuously inundated
77 area and a frequently inundated floodplain area. Based on the winter flooding inundation phenomenon in the study reach,
78 an image from 10 Mar 2015 (the day on which the winter flooding inundated area reached the annual maximum) was
79 used to divide the relatively static area into two zones: a regularly inundated floodplain area and an extremely rarely
80 inundated floodplain area. This border corresponded to an embankment road between the old floodplain area and the
81 newly formed floodplain area, which created an approximately 1 m elevation difference. Therefore, the entire study area
82 from the river to the floodplain margins was divided into four zones, including a continuously inundated area (belt 1), a
83 frequently inundated floodplain area (belt 2), a regularly inundated floodplain area (belt 3) and an extremely rarely
84 inundated floodplain area (belt 4).

85 MODIS-NDVI data source and preprocessing

86 Daily Aqua/Terra MODIS surface reflectance data (MODIS9GQ) images with the medium spatial resolution (250
87 m) were downloaded in bulk from Atmosphere Archive and Distribution System Distributed Active Archive Center
88 (LAADS DAAS) at the Goddard Space Flight Center website (<https://labsweb.modaps.eosdis.nasa.gov>) using Wget
89 software (<https://eternallybored.org/misc/wget/>). A total of 8000 images with tiles of H26V04 (horizontal number 26 and
90 vertical number 04) were downloaded for the period between 1 Jan. 2010 and 31 Dec. 2015. MODIS images were carried
91 out standard atmospheric corrections (Flood et al, 2013; Vermote et al; 2015). Data re-projected from the sinusoidal to
92 the WGS84 geographic coordinate system, images were clipped by a study area vector-border map, and before
93 downloading, the image type has been converted to the tagged image file format on the website. Subsequently, cloud-free
94 images were selected from the postprocessed images.

95 The NDVI has been used extensively to examine vegetation growth and vigor in arid floodplains (Marchetti et al,
96 2016); it was used to investigate vegetation responses to the river hydrogeomorphology in the study area. The formula
97 for the NDVI is as follows:

$$98 \quad \text{NDVI} = \frac{(\text{NIR} - \text{RED})}{(\text{NIR} + \text{RED})}$$

99 where NIR is the reflectance value of the MODIS9GQ 2-band (841-876 nm) and RED is the MODIS 9GQ 1-band
100 (620-670 nm).

101 The NDVI values range from -1 to 1, with negative values corresponding to areas that are completely open water
 102 and positive values corresponding to areas covered by green vegetation (Marchetti et al, 2016). Here, NDVI statistical
 103 indicators, including the maximum NDVI value, frequency of NDVI value and water-inundation persistence time, were
 104 used to quantify the vegetation responded to the hydro-geomorphological dynamics of the floodplains.

105 The maximum NDVI value is the highest NDVI value of each pixel in giving periods.

106 The formula is as follows:

$$P_{NM} = \text{Max} (P_{1(NDVI)}, P_{2(NDVI)}, P_{3(NDVI)}, \dots, P_{n(NDVI)})$$

107 where P_{NM} is the maximum NDVI value of pixel $_{(x,y)}$ in the images, t is the collection time of the images, and n is the
 108 number of images. The maximum value calculation model in ENVI software was used to acquire pixel-based maximum
 109 NDVI value images from daily time-series NDVI images between 1 Apr. 2015 and 31 Oct. 2015 and it was used to
 110 describe the different zonal distributions of floodplain plant phenology from the riverbed to floodplain margins.

111 The frequency of the NDVI value represents the number of repeated occurrences of a value given time range within
 112 each pixel. The formula for is as follows:

$$P_{NF} = \sum_{i=1}^n P_{(NF)} = \text{Sum} (P_{1(NF)} + P_{2(NF)} + P_{3(NF)} + \dots + P_{n(NF)})$$

113 where P_{NF} is the total occurrence times of given NDVI value in each pixel, and n is the number of images. Python was
 114 used to calculate the pixel-based occurrence times of NDVI values from 1 Jun. 2010 to 31 Dec. 2015.

115 Inundation water persistence time is the number of days in which water continues to submerge within a given time
 116 range in each pixel. This parameter can effectively describe the spatial distribution patterns of floodplain hydrology. The
 117 formula is as follows:

$$P_{WP} = \sum_{i=0}^n P_{(WP)} = \text{Sum} (P_{1(WP)} + P_{2(WP)} + P_{3(WP)} + \dots + P_{n(WP)})$$

118 where P_{WP} is the total water persistence days of each pixel in the images, and n is the number of days. Daily NDVI
 119 images from 1 Nov. 2014 to 31 Mar. 2015 and extracted daily pixel-based water areas were used in acquiring a pixel-
 120 based floodplain water-inundation persistence time map.

124 Results

125 Floodplain hydro-geomorphological dynamics

126 The hydro-geomorphology dynamics of the study area from 2010 to 2015 was analyzed by using daily average water
 127 level and MODIS-NDVI time series. The average yearly summer and winter water levels differed significantly in this
 128 period (Fig.2A), approximately 1050.69 m and 1051.61m. The average water level in winter was about 0.91m higher than
 129 in summer. There are also obvious differences between the annual average maximum water level in summer and winter.
 130 In study period, the summer maximum water level was 1051.5 m and the winter maximum water level was
 131 approximately 1053 m. The highest yearly maximum summer water level occurred in 2013 and was 1052.17 m (Fig. 2B).
 132 The monthly average, maximum and minimum water levels between 2010 and 2015 were analyzed in the study reach.
 133 The summer water levels slightly increased from July to October and comparing to the water level data of the study period,
 134 it can be seen that the data in June to October are higher than that of November and April (Fig. 2C).

135 Water-persistence times have clear zonal characteristics in which the inundation persistence time gradually decreases
 136 from the riverbed to edge of the floodplains (Fig. 3A). In the marginal zones, the persistence time of water inundation is
 137 0 day. In comparison to other places, inundated areas of the riverbed have longest persistence times, ranging from 108 to
 138 151 days. The zone between the highest persistence time of inundated areas and un-inundated areas has a persistence time
 139 ranging from 1 to 97 days.

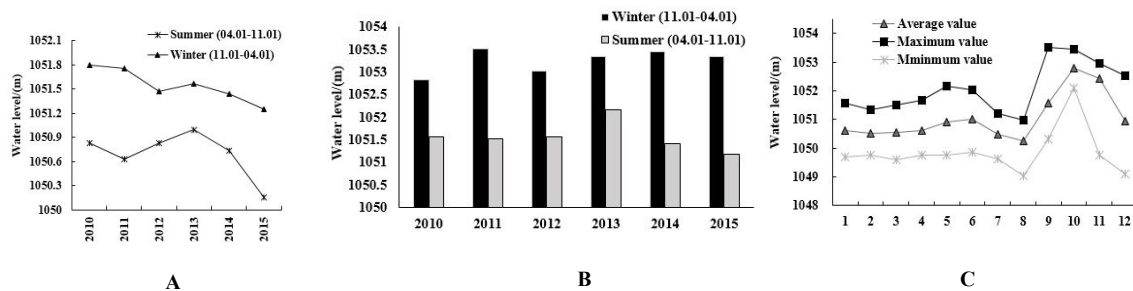


Figure 2 The intra and inter-annual hydrological regime changes of the Bayangaole water stations. (A) Yearly average winter and summer water levels in Bayangaole water station from 2010 to 2015. Winter water level is statistics from Nov.1 to the next year Apr.1 each study year; summer water level is statistics from Apr.1 to Nov.1 each study year. (B) Yearly maximum winter and summer water levels in Bayangaole water station from 2010 to 2015. Winter water level is statistics from Nov.1 to the next year Apr.1 each study year; summer water level is statistics from Apr.1 to Nov.1 each study year. (C) Monthly average, maximum and minimum water levels in Bayangaole water station from 2010 to 2015.

140 The pixels that are more frequently inundated by flood waters classified to dynamic floodplain areas, and pixels that
 141 are seldom inundated by river water in the study period are classified as static floodplain areas (Fig. 3B). The cumulative
 142 inundation area changes over time and is significantly correlated with the daily water level changes (Fig. 3C). Figure
 143 shows that daily average water levels begin to rise on 31 Nov. 2014, two days later, the inundation area appears to
 144 dramatically increase and reaches its highest value.

145 Temporal difference of vegetation dynamics

146 Pixel-based time-series NDVI from 1 Jun. 2010 to 31 Dec. 2015 were used to illustrate the vegetation response to
 147 floodplain hydrogeomorphology, floodplain hydrogeomorphology significantly static during this period. Therefore, based

148 on the conceptual zonal distributions in each zone, one point (pixel) was chosen for a total of four points located along a
 149 cross section with different distances to the riverbed: 0 km (P1), 0.2 km (P2), 0.9 km (P3) and 2.2 km (P4) (Fig. 1C). P1
 150 is located in mostly inundated water and near the average centerline of the river. This point is almost continually
 151 submerged by water (Fig. 4). The NDVI value for this point is highly dynamic during the entire study period and does
 152 not show obvious interannual changes (Fig. 4A). P2 is located in the riverbed and presents a vertical distance of 0.2 km
 153 from the river. This zone has a very active river hydrology, and the NDVI curve shows similar trends to the trend for P1;
 154 thus, P2 is irregular and does not present obvious interannual changes. The vegetation type is mainly grass (Fig.4B). P3
 155 is located at a vertical distance of 0.9 km from the river, and although it is less affected by regular summer river
 156 hydrological changes, it is regularly inundated by spring and autumn overbanked water caused by winter ice floods. P3
 157 has a regular NDVI curve as well as distinctly higher NDVI values. The figure showing interannual changes indicates
 158 that the NDVI of P3 begins to gradually increase from Apr. and reaches its highest values between Jul. and Oct.; moreover,
 159 clear differences from the other NDVI trends are observed. Furthermore, the NDVI values are less than 0 from Dec. to
 160 Mar. each year (Fig.4C). P4 is located in the marginal zone of the floodplain at the farthest distance from the riverbed
 161 (2.3 km). This point has not been submerged by flooding since the large flooding (5800 m³/s) event that occurred on 24
 162 Aug. 1989. The NDVI curve of P4 presents regular dynamics, and the NDVI values show considerable increases from
 163 Jun. to Sep. The peak NDVI value is not as high as that of P3, and values less than 0 are not observed throughout the
 164 study period (Fig.4D).

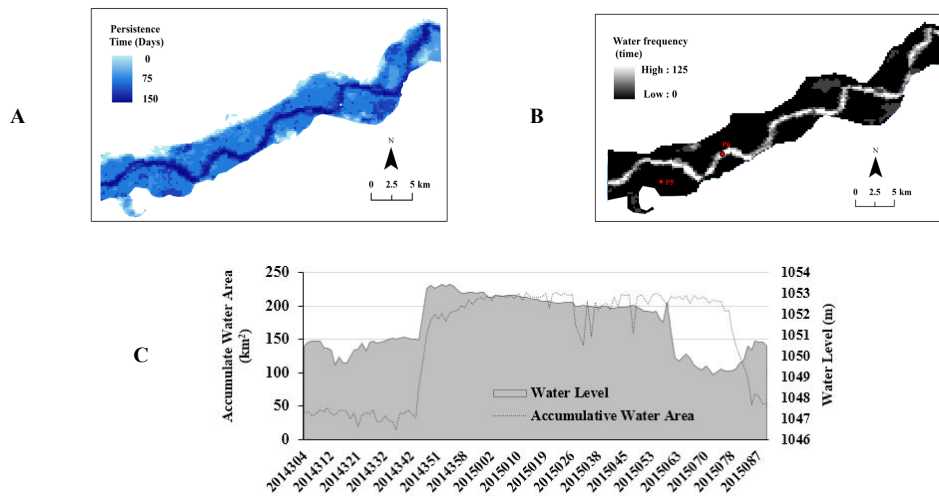


Figure 3 Spatiotemporal distribution patterns of water persistence time and frequency. (A) Floodplain water inundation persistence time map in study area from 1 Nov. 2014 to 31 Mar. 2015. (B) Pixel based water frequency images in study area from 2010 to 2015 (from 1 Apr. to 1 Nov. in each year). P5 at the static geomorphological area, P6 at the highly dynamic geomorphological area. (C) Cumulative water inundation area and daily water levels in the study area from 1 Nov. 2014 to 1. Apr 2015.

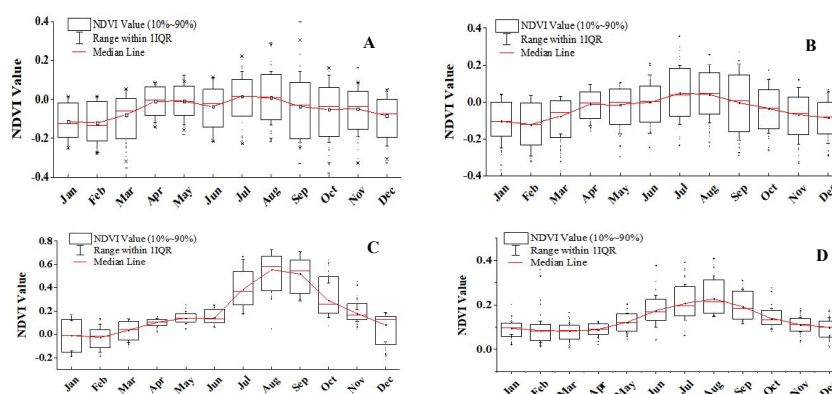


Figure 4 Inter-annual changes in the NDVI curves of different points from the riverbed to the edge of floodplain. A At the riverbed, B distance of 0.2 km to the riverbed, C distance of 0.9 km to the riverbed, and D distance of 2.2 km to the riverbed

Spatial distribution difference of vegetation

165 The maximum value calculation model in ENVI software was used to acquire pixel-based peak NDVI value images
 166 from daily multiband NDVI images between 1 Apr. 2015 and 31 Oct. 2015. The entire study area was divided into four
 167 zones based on the different spatial distribution patterns of peak NDVI values. The peak NDVI values, which are less
 168 than 0.2, are mainly distributed in the riverbed area in regions P1 and P2, whereas the highest peak NDVI values, which
 169 are greater than 0.4, occur in the P3 region. Peak NDVI values of the marginal plain zones in region P4 are between 0.3
 170

171
172
173
174
175

and 0.4, and this region presents a clear border with the zone that contains the highest peak NDVI values throughout the study area. (Figs. 5A-B)

Python was used to calculate the pixel-based frequency occurrence times of NDVI values from 1 Jun. 2010 to 31 Dec. 2015 as follows: >0 , $0-0.1$, $0.1-0.2$, $0.2-0.3$, $0.3-0.4$, $0.4-0.5$, and $0.5-0.6$ and <0.6 . In the maps, blue pixels represent high-frequency NDVI values, and green ones represent low-frequency NDVI values. A map of the spatial distributions

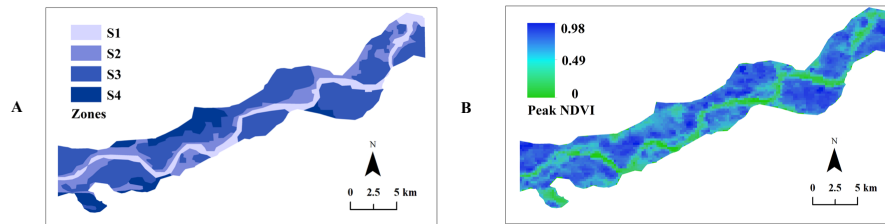


Figure 5 Spatial distribution patterns of the peak NDVI values in study area (A) and categories of different zones (B)

176
177
178
179
180
181
182
183
184
185
186
187
188
189
190
191
192
193
194
195

of the frequencies of NDVI values less than 0. The frequencies of NDVI values that were less than 0 were mostly concentrated in the riverbed zone (Fig. 6A). The frequency results for NDVI values between 0 and 0.1. High-frequency NDVI values mainly appeared in the riverbed, and some appeared in the floodplain margins (Fig. 6B). The spatial distribution map with the frequency of NDVI values between 0.2 and 0.3. Except for the riverbed zone, the other zones included other frequency NDVI values, and the high-frequency values were mainly distributed in the floodplain margins. Spatial distribution patterns were characterized by gradually increasing values from the riverbed to the floodplain margins (Fig. 5C). The spatial distribution maps of the frequencies of NDVI values with ranges between 0.3 and 0.4 and between 0.4 and 0.5. High-frequency values mostly appeared in the marginal areas of the floodplain (Figs. 6D-F). The high NDVI values were mainly distributed in the zone between the riverbed and the floodplain margins between ranges from 0.5 to 0.6 and values greater than 0.6. (Figs. 6G-H). The frequency of different NDVI values was calculated for four points: P1, P2, P3 and P4 (Figs. 7A-D). Fig. 7A represents P1 and has a total frequency of NDVI values of 1490 times. The frequency of NDVI values less than 0.1 is 1448, which is 97.1% of the total. The frequency of NDVI values less than 0 is the dominant NDVI value at P1, with a frequency of 1071. Fig. 7B represents P2, which has a frequency of NDVI values between 0.1 and 0.3, which is double that of P1. A frequency between 0.3 and 0.4 occurred once. Fig. 7C represents P3, which is located in the regularly flooded zone. The highest frequency of NDVI values was between 0.1 and 0.2. The frequency of NDVI values greater than 0.3 is higher at this point than the other three points. NDVI values greater than 0.4 do not occur at the other three points, although NDVI values less than 0 are observed at this point mainly because of the ice jam phenomenon that occurs every winter. P3 is covered by water or ice in winter. Fig. 7D represents P4, the farthest point from the riverbed. NDVI values less than 0 only occur 3 times, and the frequency range from 0 to 0.3 encompasses 95% of the total.

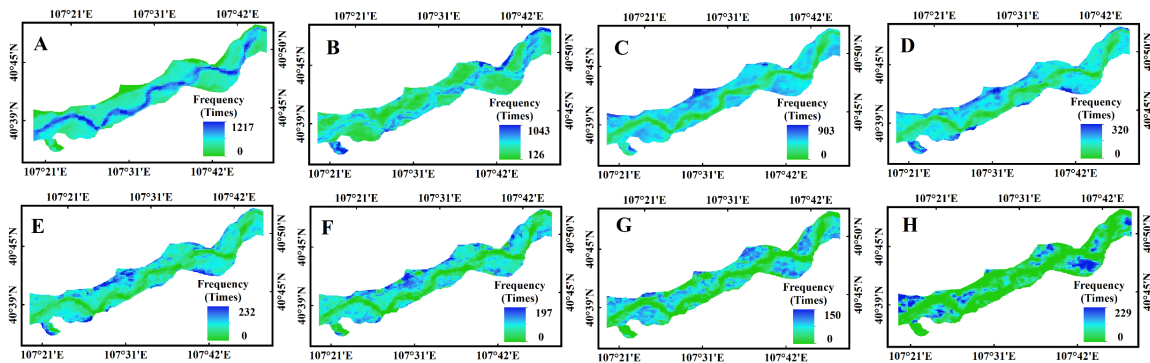


Figure 6 Pixel based spatial distribution patterns of the NDVI frequency. (A) Frequency <0 , (B) frequency $0-0.1$, (C) frequency $0.1-0.2$, (D) frequency $<0.2-0.3$, (E) frequency $<0.3-0.4$, (F) frequency $<0.4-0.5$, (G) frequency $<0.5-0.6$, and (H) frequency >0.6

196
197
198
199
200
201
202
203
204
205
206
207
208

Floodplain vegetation response to hydro-geomorphological dynamics

Based on NDVI values less than 0, river hydrology persistence time was quantified to identify relationships between hydrology and vegetation growth in each pixel of the floodplain. Moderate Resolution Imaging Spectroradiometer (MODIS) images were used to remove the water (including ice and snow) area from 1 Nov. 2014 to 31 Mar. 2015. A correspondence analysis was then performed on the daily water levels and the daily cumulative water-inundation area of the study area.

The spatial distribution of persistence times of the inundated water area is highly related to the spatial distribution of NDVI frequencies and peak NDVI values (Figs. 2A, 4 and 5). A spatial distribution of persistence times of inundated water areas between 108 and 151 corresponds to peak NDVI values less than 0.1, and a high frequency of NDVI values less than 0.1 is observed in this region. The zone has a persistence time of water-inundation areas between 1 and 100 days. The peak NDVI values of this zone are mostly larger than 0.4, and the highest frequency of NDVI values is greater than 0.3. The area with 0 water persistence time in submerged area is located at the edge of floodplain, its NDVI peak value is between 0.2 and 0.3, and the highest frequency of NDVI values is between 0.1 and 0.3.

Pixel-based peak-NDVI values of the four points from 2010 to 2015 (from 1 Apr. to 31 Oct.) and water persistence time from 2010 to 2015 (from 1 Nov. to 31 Mar.) were used to establish a simple linear regression model between the

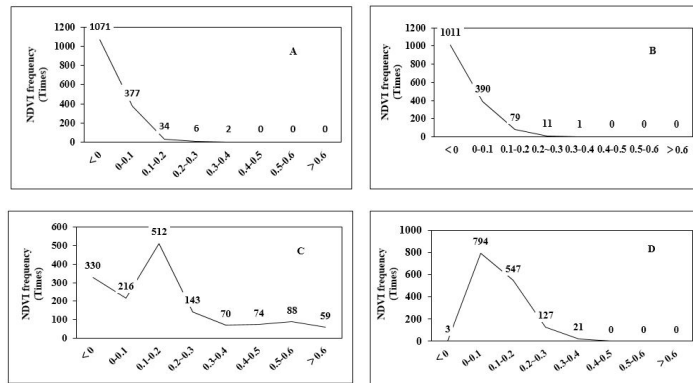


Figure 7 Statistics of each NDVI frequency ranges in different points from the riverbed to the edge of floodplain. (A) Different NDVI frequency range for point 1 in highly active permanent inundation zone, (B) different NDVI frequency range for point 2 in the highly active frequency inundation area, (C) different NDVI frequency range for point 3 in the static regular inundation area, and (D) different NDVI frequency range for point 4 in the static extremely rare inundation area.

yearly average peak NDVI values and the yearly winter high-water persistence times (Fig. 7). A good correlation coefficient is observed between the peak NDVI values of points located in the regular zone with water persistence times between 1 and 100 days (the correlation coefficient is 0.84 at a 1% significant level). The peak NDVI values of the other points are not well correlated with the persistence time of winter water levels.

Pixels P5 and P6 were selected from the dynamic area and static area, respectively (Fig. 9A). P5 was extracted from a stable area, and the NDVI curve of this pixel for the study period appeared to show more regular dynamic changes. P6 was extracted from a highly active floodplain zone, and its NDVI curve appeared irregular. Thus, the dynamic area presents lower peak NDVI values than the static area (Fig. 9B) at 0.4 and greater than 0.6, respectively. The range variations in peak NDVI values are less in the dynamic area (less than 0.2) than in the static area (between 0.1 and 0.7).

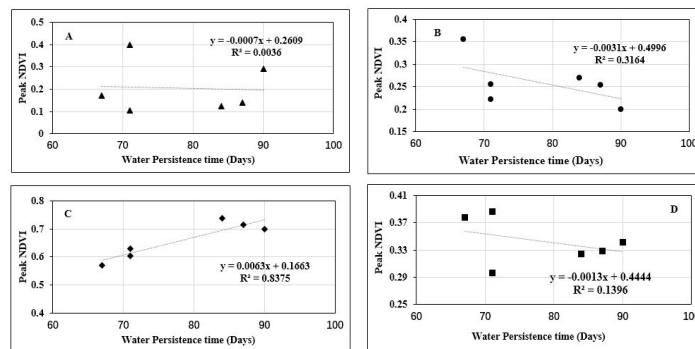


Figure 8 Regression analysis between the daily water level and peak NDVI value at different points. (A) for point 1 in highly active permanent inundation zone, (B) for point 2 in the highly active frequency inundation area, (C) for point 3 in the static regular inundation area, and (D) for point 4 in the static extremely rare inundation area.

Discussion

Vegetation is one of the most important elements of floodplains in arid and semiarid regions^{1,5}, and its response to floodplain hydrogeomorphology has attracted increasing attention in recent decades (Hupp et al, 1983,1986; Osterkamp, 1998). However, there is a topic that has not been well studied is the development of a method for quantifying differences in floodplain vegetation responses to changes in hydrogeomorphology from the riverbed to the edges of floodplains in high-latitude arid regions using MODIS time series. In this study, the different summer and winter hydrological dynamics of floodplain were analyzed, the specific quantitative information was provided on different responses of floodplain

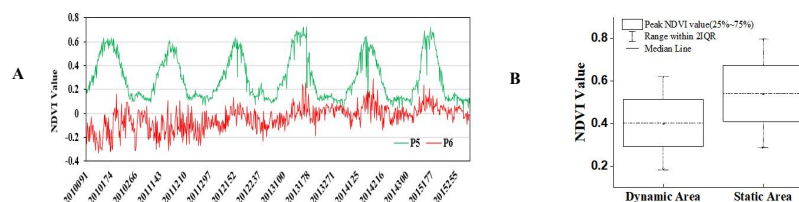


Figure 9 Spatiotemporal geomorphological dynamics of study area(A) NDVI curves in different geomorphology units. P5 at the static geomorphological area, P6 at the highly dynamic geomorphological area; (B)Box chart of the NDVI values in the highly dynamic and static geomorphological areas

227 vegetation to hydrogeomorphology from the riverbed to floodplain margins and the hydro-geomorphology changing
228 patterns that benefit to the growth and biomass of floodplain vegetation were revealed. This information plays a key role
229 for improving the management of surface water resources and preserving or extending floodplain vegetation
230 (Cunningham et al, 2013; Murray Darling Basin Authority, 2014).

231 Recent conceptual models about floodplain vegetation and river hydro-geomorphological interactions provide potential
232 methods for quantifying vegetation responses to floodplain hydro-geomorphological dynamics. Gurnell et al. (2016)
233 proposed an explicit conceptual model of vegetation and hydro-geomorphological interactions within river corridors.
234 They defined five dynamic river zones within which different hydro-geomorphological processes occur and the dominant
235 plants and physical processes interact in different ways. However, this conceptual model was just developed within a
236 European context. The hydrological factors only included flooding, while the different effects from the seasonal (summer
237 and winter) flooding on the zonal distribution of floodplain hydro-geomorphological characteristics were not considered.
238 In our study, based on the previous conceptual models and considering the impacts of ice flooding on the floodplain
239 vegetation in high-latitude arid regions combined with different hydrological patterns in summer and winter and also
240 active channel dynamics, the study area was divided into four different hydro-geomorphological characteristic zones.
241 Marchetti et al. (2016) used 16-day MODIS-NDVI time-series data to characterize floodplain geomorphological
242 dynamics. They used NDVI as an indicator of floodplain geomorphological activities, and based on the NDVI diversity,
243 the study reach was divided into highly active and static geomorphologic belts. In this study, based on the different
244 floodplain hydro-geomorphological characteristics, static and highly active geomorphologic areas in the floodplain with
245 different hydrological characteristics were identified, and these two areas were further divided into four zones, including
246 a highly active permanent water area, highly active frequently inundated area, static water inundation area, and static
247 extremely rarely inundated area. Vegetation from the riverbed to floodplain margins had a different response to river
248 hydrogeomorphology in these four zones. Broich et al. (2018) used time-series remote-sensing images based on a
249 statistical modeling approach to quantify the relationship between Australia's dryland vegetation and flooding dynamics
250 during dry and wet periods, but this quantification approach and the data sources strongly suffered by regional limits and
251 cannot be applied to river floodplains in the high-latitude arid regions, especially floodplains occurs to the ice flooding
252 phenomenon.

253 Remote sensing represents unparallel tool for investigating floodplain vegetation and river hydro-geomorphology in
254 arid regions (Marchetti et al, 2013; Mohammadi et al, 2017). For highly dynamic, wandering river floodplains, performing
255 field surveys or historical mapping to capture the short-term dynamics of floodplains presents high costs, and obtaining
256 highly dynamic detailed characteristics of large-scale floodplain areas is difficult with these techniques. High-revisit
257 remote-sensing images can fill this gap (Tucker, 1979; Raclot, 2006). Our study was based on MODIS9GQ daily NDVI
258 images with a 250 m spatial resolution, and a pixel-based analysis of the vegetation dynamics from the riverbed to the
259 edge of the floodplain was performed. Although the vegetation response to river hydrology and geomorphology using
260 remote-sensing technology has been previously debated (Marchetti et al, 2013; Mohammadi et al, 2017), and provided
261 more thorough about quantification of vegetation growth and biomass using NDVI time-series statistical indicators, such
262 as maximum NDVI value and NDVI frequency. Pixel-based differences in water-inundation persistence times in each
263 floodplain hydro-geomorphological zone were spatially quantified to provide more direct information about the spatial
264 distribution characteristics of floodplain vegetation-hydro-geomorphology from the riverbed to the edge of floodplain.
265 Mohammadi et al.(2017), based on MODISGA images, used time series of remotely sensed normalized difference water,
266 vegetation and moisture indices to characterize extinction floodplain dynamics and indicated that this approach provides
267 a complementary tool for ecological studies of floodplain productivity, which mainly have utilized vegetation indices to
268 understand the spatiotemporal effects of flooding on productivity. However, as in the present study, their study area
269 included few vegetation canopies or types (in our study area, most of the floodplain was covered by herbs) and involved
270 medium-sized floodplains, making it impossible to demonstrate the difference in spatial distributions using low spatial-
271 resolution remote-sensing images, such as a 500 m spatial resolution. Therefore, MODIS-NDVI time series with a 250 m
272 spatial resolution also has more potential value for quantifying the vegetation growth and biomass of these areas in
273 response to floodplain hydro-geomorphological dynamics. Our research also shows for the first time the differences in
274 vegetation zone distribution patterns of the wandering reach floodplains of the Yellow River and the results can provide
275 insights to improve the management of the Yellow River floodplains located in high-latitude arid regions.

276 **Conclusions**

277 Time-series daily MODIS-NDVI images were used to quantify pixel-based floodplain vegetation responses to
278 changes in floodplain hydrogeomorphology from a riverbed to the edge of the floodplain in a high-latitude arid region.
279 Using remote-sensing time-series NDVI statistical indices, including the frequency of NDVI values, peak NDVI value
280 and water persistence time, to quantify highly dynamic wandering rivers in arid regions represents a considerable advance
281 and provides direct information to quantify floodplain vegetation responses to hydrogeomorphology. Floodplain
282 vegetation has obvious spatial zonal distribution characteristics from the riverbed to the edge of floodplain, and vegetation
283 growth and biomass were mainly controlled by floodplain hydrogeomorphology. The regression analysis between the
284 water persistence times and peak NDVI values showed that regular water inundation is better than high-frequency or
285 extremely rare inundation rates for floodplain vegetation growth. Within regular water persistence time scales, increasing
286 the water-inundation time is beneficial for vegetation growth in regularly inundated static areas. Our research reveals
287 potential advantages for the use of remote sensing to investigate floodplain vegetation, and these results can be referenced
288 to manage wandering river floodplains located in high-latitude arid regions.

References

1. Azzali, S., M. Menenti (2000) Mapping vegetation-soil-climate complexes in southern Africa using temporal Fourier analysis of NOAA-AVHRR NDVI data. *International Journal of Remote Sensing* 21(5): 973-996. Doi: 10.1080/014311600210380
2. Broich, M., M. G. Tulbure, J. Verbesselt, Q. Xin, J. Wearne (2018) Quantifying Australia's dryland vegetation response to flooding and drought at sub-continental scale. *Remote Sensing of Environment* 212: 60-78. Doi: 10.1016/j.rse.2018.04.032
3. Capon, S. J (2003) Plant community responses to wetting and drying in a large arid floodplain. *River Research and Applications* 19(5-6): 509-520. Doi: 10.1002/rra.730
4. Capon, S. J (2005) Flood variability and spatial variation in plant community composition and structure on a large and floodplain. *Journal of Arid Environments* 60(2): 283-302. Doi: 10.1016/j.jaridenv.2004.04.004
5. Cunningham, S., White, M., Griffioen, P., Newell, G., Mac Nally, R., 2013. Mapping Floodplain Vegetation Tyoes across the Murray-Darling Basin Using Remote Sensing. Murray Darling Basin Authority, Canberra.
6. Epting, J., D. Verbyla, B. Sorbel (2005) Evaluation of remotely sensed indices for assessing burn severity in interior Alaska using Landsat TM and ETM+. *Remote Sensing of Environment* 96(3-4): 328-339. Doi: 10.1016/j.rse.2005.03.002
7. Gurnell, A. M., R. C. Grabowski (2016) Vegetation-Hydrogeomorphology Interactions in a Low Energy, Human-Impacted River. *River Research and Applications* 32(2): 202-215. Doi:10.1002/rra.2922
8. Hamilton, S. K., J. Kellndorfer, B. Lehner, M. Tobler (2007) Remote sensing of floodplain geomorphology as a surrogate for biodiversity in a tropical river system (Madre de Dios, Peru). *Geomorphology* 89(1-2): 23-38. Doi: 10.1016/j.geomorph.2006.07.024
9. Hupp, C. R (1983) Vegetation Pattern on Channel Features in the Passage-Creek Gorge, Virginia. *Castanea* 48(2): 62-72.
10. Hupp, C. R (1986) UPSTREAM VARIATION IN BOTTOMLAND VEGETATION PATTERNS, NORTHWESTERN VIRGINIA. *Bulletin of the Torrey Botanical Club* 113(4): 421-430. Doi: 10.2307/2996435
11. Landmann, T., M. Schramm, R. R. Colditz, A. Dietz, S. Dech (2010) Wide Area Wetland Mapping in Semi-Arid Africa Using 250-Meter MODIS Metrics and Topographic Variables. *Remote Sensing* 2(7): 1751-1766. Doi:10.3390/rs207175.
12. Makkeasorn, A., N.-B. Chang, J. Li (2009) Seasonal change detection of riparian zones with remote sensing images and genetic programming in a semi-arid watershed. *Journal of Environmental Management* 90(2): 1069-1080. Doi: 10.1016/j.jenvman.2008.04.004
13. Marchetti, Z. Y., P. G. Minotti, C. G. Ramonell, F. Schivo, P. Kandus (2016) NDVI patterns as indicator of morphodynamic activity in the middle Parana River floodplain. *Geomorphology* 253: 146-158.
14. Mohammadi, A., J. F. Costelloe, D. Ryu (2017) Application of time series of remotely sensed normalized difference water, vegetation and moisture indices in characterizing flood dynamics of large-scale arid zone floodplains. *Remote Sensing of Environment* 190: 70-82. Doi: 10.1016/j.rse.2016.12.003
15. Murray Darling Basin Authority, 2014. Basin-wide Environmental Watering Strategy. Murray Darling Basin Authority, Canberra.
16. Neuenschwander, A. L., K. A. Crews (2008) Disturbance, management, and landscape dynamics: Harmonic regression of vegetation indices in the lower Okavango Delta, Botswana. *Photogrammetric Engineering and Remote Sensing* 74(6): 753-764. Doi:10.14358/PERS.74.6.753
17. Osterkamp, W. R (1998) Processes of fluvial island formation, with examples from Plum Creek, Colorado and Snake River, Idaho. *Wetlands* 18(4): 530-545. Doi: 10.1007/BF03161670
18. Raclot, D (2006) Remote sensing of water levels on floodplains: a spatial approach guided by hydraulic functioning. *International Journal of Remote Sensing* 27(12): 2553-2574. Doi:10.1080/01431160600554397
19. Sims, N. C., M. J. Colloff (2012) Remote sensing of vegetation responses to flooding of a semi-arid floodplain: Implications for monitoring ecological effects of environmental flows. *Ecological Indicators* 18: 387-391.
20. Tucker, C. J (1979) Red and Photographic Infrared Linear Combinations for Monitoring Vegetation. *Remote Sensing of Environment* 8(2): 127-150. Doi: 10.1016/0034-4257(79)90013-0
21. Tockner, K., J. A. Stanford (2002) Riverine flood plains: present state and future trends. *Environmental Conservation* 29(3): 308-330. Doi: 10.1017/S037689290200022X
22. Thomas, R. F., R. T. Kingsford, Y. Lu, S. J. Cox, N. C. Sims, S. J. Hunter (2015) Mapping inundation in the heterogeneous floodplain wetlands of the Macquarie Marshes, using Landsat Thematic Mapper. *Journal of Hydrology* 524: 194-213. Doi: 10.1016/j.jhydrol.2015.02.029